

# VIPA: Visual Informative Part Attention for Referring Image Segmentation

Yubin Cho, Hyunwoo Yu, Kyeongbo Kong, Kyomin Sohn, Bongjoon Hyun and Suk-Ju Kang, *Member, IEEE*

**Abstract**—Referring Image Segmentation (RIS) aims to segment a target object described by a natural language expression. Existing methods have evolved by leveraging the vision information into the language tokens. To more effectively exploit visual contexts for fine-grained segmentation, we propose a novel Visual Informative Part Attention (VIPA) framework for referring image segmentation. VIPA leverages the informative parts of visual contexts, called a visual expression, which can effectively provide the structural and semantic visual target information to the network. This design reduces high-variance cross-modal projection and enhances semantic consistency in an attention mechanism of the referring image segmentation. We also design a visual expression generator (VEG) module, which retrieves informative visual tokens via local-global linguistic context cues and refines the retrieved tokens for reducing noise information and sharing informative visual attributes. This module allows the visual expression to consider comprehensive contexts and capture semantic visual contexts of informative regions. In this way, our framework enables the network’s attention to robustly align with the fine-grained regions of interest. Extensive experiments and visual analysis demonstrate the effectiveness of our approach. Our VIPA outperforms the existing state-of-the-art methods on four public RIS benchmarks.

**Index Terms**—Visual informative part attention, Visual expression, Referring segmentation.

## I. INTRODUCTION

Referring image segmentation (RIS) [1]–[3] is one of the challenging vision-language tasks and can be applied in various applications such as human-robot interaction and the object retrieval. Given an image and a natural language expression describing a target object within the image, the key point in this task is for the network to precisely segment the target object regions from the image by referencing the given target information.

As shown in Figs. 1 (a) and (b), the role of a Transformer decoder differs for a certain purpose. Previous RIS methods [4]–[6] have adopted a Transformer-based segmentation decoder using vision features as queries and language tokens as keys-values to find the target regions by referencing the given language information. As a key-value set, some studies

Yubin Cho and Hyunwoo Yu contributed equally to this work. (Corresponding author: Suk-Ju Kang.)

Yubin Cho was with the School of Artificial Intelligence, Sogang University (e-mail: dbqls1219@sogang.ac.kr) and she is currently with the AI Lab of CTO division, LG Electronics (e-mail: ubin.cho@lge.com).

Hyunwoo Yu, and Suk-Ju Kang are with the School of Electronic Engineering, Sogang University (e-mail: hyunwoo137@sogang.ac.kr; sjkang@sogang.ac.kr).

Kyeongbo Kong is with the School of Electronic Engineering, Pusan University (e-mail: kbkong@pusan.ac.kr).

Kyomin Sohn and Bongjoon Hyun are with the Memory Business Division, Samsung Electronics (e-mail: kyomin.sohn@samsung.com; bongj.hyun@samsung.com).

[5], [7]–[14] use the advanced language tokens extracted by the bidirectional cross-attention encoders to enhance alignment with cross-modal information. More recent studies [6], [15]–[17] employ LLMs [18], [19] to improve understanding of the language expression via LLM’s immense knowledge, and exploit the generated language tokens in the segmentation decoder, as shown in Fig. 1(b).

In this task, we found that how to construct the key-value information when the query is the vision feature in the segmentation decoder has a significant impact on segmentation performance. Based on this perspective, the general RIS framework can be interpreted as that the informative tokens (*e.g.*, language tokens in previous methods) regarding the target object are leveraged as a key-value set to assign attention to target regions for vision query features. In other words, the role of the key-value set is a target information provider that guides the network on which regions to focus its attention. However, there is an inherent limitation of RIS task *i.e.*, target information is only given by a free-form language input, which has been noted in failure cases of prior works [20], [21]. Previous works using visual-aware language tokens as a key-value set have achieved performance improvements by leveraging the visual information into the language tokens. Inspired by these works, we explore the following key questions: *What is the effective key-value set for providing semantic target information to vision query features in the segmentation network? How can we leverage the visual information more effectively for fine-grained segmentation?*

We propose a novel Visual Informative Part Attention (VIPA) framework to more effectively exploit visual contexts for referring image segmentation. VIPA framework aligns the query and key-value representations within the visual modality, thereby reducing the high-variance cross-modal projection and enhancing semantic consistency in the attention mechanism. Specifically, VIPA leverages the retrieved informative parts of visual contexts as a key-value set for the vision query features in the Transformer-based segmentation decoder; such informative parts of visual contexts are called *Visual Expression* in this paper. We explore the linguistic context-relevant retrieved parts of visual tokens for visual expression, since the given linguistic context is inherently involved with target information. These informative parts of visual contexts contain more structural and semantic target information that is crucial for fine-grained segmentation. Hence, the visual expression robustly leads the network’s attention to the region of interest by providing semantic visual target contexts to the network on this task. As shown in Fig. 1(c), the network’s attention by language-based tokens tends to miss the target regions or attend to even wide non-target regions. In contrast, our VIPA

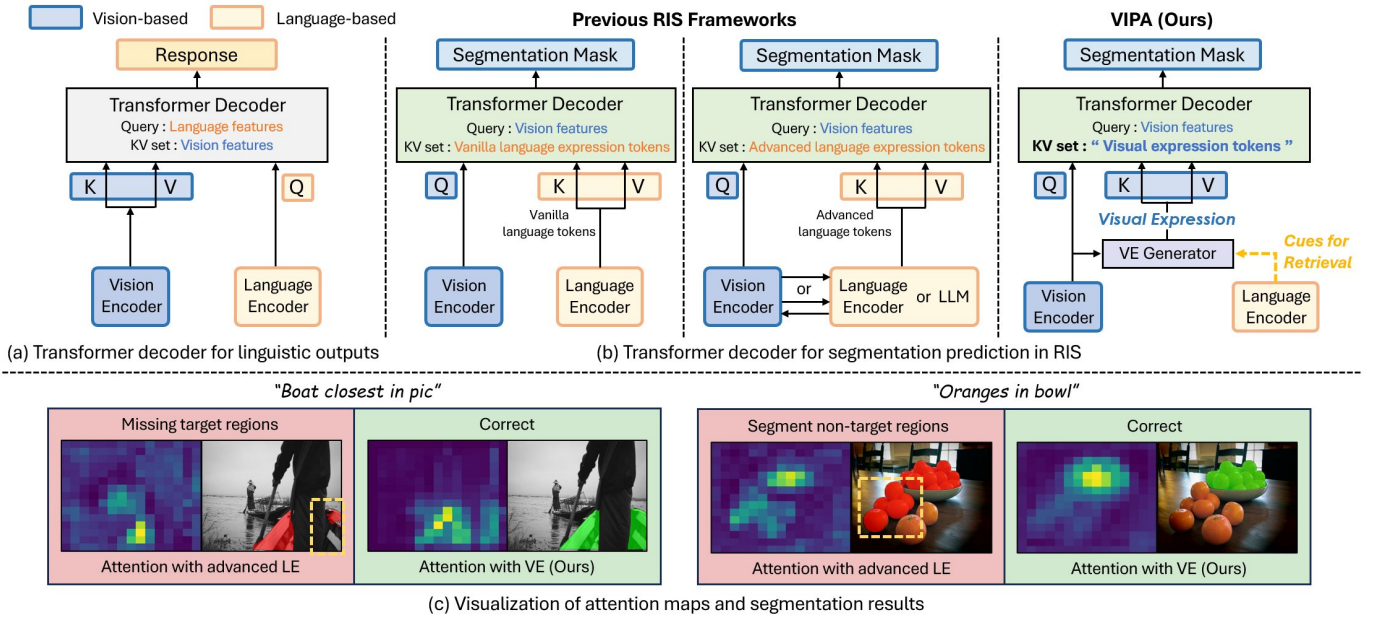


Fig. 1: (a) Example of a transformer decoder used to extract language outputs. (b) Illustration of different RIS frameworks. Different from previous works, our approach leverages *visual expression*, generated from the retrieved informative parts of visual contexts, as a key-value set in the Transformer-based segmentation decoder. (c) Visual comparison of two different key-value sets. Yellow dotted boxes are incorrect predictions. The visual expression (VE) robustly guides the network’s attention to the regions of interest by enhancing semantic coherence in the attention mechanism of referring image segmentation, whereas the advanced language expression (LE) results in incomplete predictions.

facilitates alignment between the network’s attention and the fine-grained region of interest. These observations indicate that our visual expression approach leverages visual information more effectively rather than the prior approach projecting visual information into language tokens. To the best of our knowledge, VIPA approach is the first to explicitly explore the informative parts of visual contexts as a key-value set for an advanced information provider in the attention mechanism of the referring image segmentation.

We also design a visual expression generator (VEG) module for informative visual expression. Firstly, this module leverages local-global linguistic contexts as cues to retrieve the informative visual tokens among all visual tokens, because most visual pixels in the image are not in the region of interest. The [CLS] token and word tokens of language features contain the global (*i.e.*, sentence-level) context and the local (*i.e.*, word-level) context of each word, respectively. By exploiting these local-global contexts, the visual expression can consider both the comprehensive context and the attribute contexts for the target object. Secondly, our module implements the visual context refinement step to ensure the informativeness of visual expression tokens. In this step, the retrieved visual tokens are refined to mitigate the possibility of being distracted by noise information and share visual attributes with each other for more attention to be devoted to semantic information. By doing so, the visual expression generated from the retrieved informative visual tokens serves as an effective key-value set in the Transformer-based segmentation decoder.

The effectiveness of VIPA is validated through comprehensive visual analyses and extensive experiments across four

public RIS benchmarks. In particular, Fig. 6 (c) demonstrates that the visual expression provides key-value representations that are aligned in the visual feature space of the query, resulting in lower modality projection entropy compared to the language-based key-value set.

Our contributions can be summarized as follows:

- We propose a novel Visual Informative Part Attention (VIPA) framework for referring image segmentation, which leverages the informative parts of visual contexts as a key-value set for the vision query features in the Transformer-based segmentation decoder. Our approach is the first to explore the potential of visual expression in the attention mechanism of the referring segmentation.
- We design a visual expression generator module, which retrieves informative visual tokens via local-global linguistic cues and refines them for mitigating the distraction by noise information and sharing the visual attributes. This module enables visual expression to consider comprehensive contexts and capture semantic visual contexts for fine-grained segmentation.
- VIPA consistently shows strong performance on four RIS benchmarks. The visual analysis of attention results clearly demonstrates the effectiveness of our approach.

## II. RELATED WORKS

### A. Referring Image Segmentation

Unlike single-modal semantic segmentation methods [22]–[27] that operate on predefined categories, referring image

segmentation (RIS) tackles the challenge of grounding unconstrained natural-language expressions to corresponding visual regions. Since the goal of RIS is to detect and segment the target object specified by language, a variety of approaches have focused on strengthening cross-modal alignment. Contrastive learning has proven particularly effective for aligning visual and linguistic representations by pulling positive pairs closer while pushing negative pairs apart. CRIS [4] extends the contrastive loss used in CLIP to a pixel-level formulation, introducing a text-to-pixel contrastive loss. CrossVLT [28] applies contrastive loss at multiple encoder stages, utilizing rich intermediate visual-linguistic cues to further enhance alignment. CGFormer [29] incorporates a contrastive objective between learnable tokens and linguistic tokens, enabling the model to identify referent-related tokens and generate their corresponding segmentation masks.

In addition to contrastive-based alignment, several structural designs have been proposed to improve cross-modal feature interaction. Some studies [30], [31] fused language features and CNN-based visual features through concatenation. CMSA [32] concatenates vision-language features and adopts self-attention to capture long-range dependencies. Transformer-based methods [7], [33]–[35] perform fusion by applying cross-attention modules to the final features of the vision-language encoder, enabling cross-modal interaction between visual and linguistic representations. However, these models typically perform fusion only on the final encoder features, failing to fully exploit rich intermediate information within the encoder. To address this limitation, early-fusion approaches [28], [36] integrate cross-attention deeper inside the encoder, thereby improving cross-modal feature fusion. In addition, methods that follow the mask-decoder framework [10], [37], [38] generate query tokens from language-guided tokens and use them to extract mask features for final prediction.

More recent studies [6], [15]–[17] employed large language models (LLMs) to improve language understanding. LISA [6] was the first model to utilize the generated linguistic token by the LLM as a key-value in the segmentation decoder. Following its success, subsequent works [39], [40] incorporate multiple LLM-generated tokens to further enrich language-guided reasoning. In parallel, several SAM-based frameworks [16], [41] have also been proposed to enhance cross-modal interaction in referring image segmentation. However, although these methods generally demonstrate strong performance, they suffer from significant overhead due to the large model size and substantial computational cost.

Our work is motivated by the observation that effective cross-modal feature fusion is crucial for RIS performance. Rather than exploring where to place cross-attention, as in prior work, we instead examine the internal design of the cross-attention mechanism and its impact on cross-modal alignment and segmentation.

### B. Attention Mechanism in Referring Image Segmentation

With the advancement of Transformers, cross-modal alignment methods based on the cross-attention mechanism have

emerged in various vision-language tasks. In referring image segmentation, VLT [7] first introduced a Transformer-based architecture to extract vision-aware language query vectors that capture diverse comprehension of language expression. They used these language vectors in the mask decoder for target segmentation.

Recent RIS studies have explored Transformer-based referring image segmentation (RIS) architectures in which visual features, as queries, reference target-informative tokens as a key-value set in the segmentation decoder. LAVT [36] employed cross-attention within the vision encoder, which uses language features as a key-value set. CRIS [4] used the vanilla linguistic features as key-value elements in the Transformer decoder for segmentation. LQMFormer [42] utilized learnable tokens, which are fine-tuned based on language expression, to extract diverse linguistic representations. Several methods [5], [11]–[13], [20], [28], [29], [43], [44] exploited the advanced linguistic features as a key-value set, which are extracted by bidirectional cross-attention to enhance the alignment between cross-modal information. CGFormer [29] used the advanced language tokens as keys-values by projecting visual information into learnable tokens conditioned on language features.

Different from previous works, our framework leverages the retrieved informative visual tokens (*i.e.*, visual expression) as a key-value set for visual informative part attention in the Transformer-based segmentation decoder, rather than projecting visual information into language tokens. By directly providing semantically and structurally rich visual contexts of the fine-grained target regions, the visual expression robustly guides the network’s attention toward the region of interest.

## III. METHOD

We propose a novel Visual Informative Part Attention (VIPA) framework for referring image segmentation, as illustrated in Fig. 2. We first describe a vision and language feature extraction, and then introduce a visual expression generator. Finally, we explain a segmentation decoder.

### A. Vision and Language Feature Extraction

Given an image  $\mathcal{I}$  and a linguistic expression  $\mathcal{L}$  that consists of  $L - 1$  words, a vision encoder extracts the vision features  $F_i \in \mathbb{R}^{H_i W_i \times C_i}$  at each stage  $i \in \{1, 2, 3, 4\}$  and a language encoder extracts the linguistic expression tokens  $E_{\mathcal{L}} = [l_{cls}, l_1, \dots, l_{L-1}] \in \mathbb{R}^{L \times D}$ . Note that  $H_i$ ,  $W_i$ ,  $C_i$  and  $D$  denote the height, width, channel dimension of the feature maps at the  $i^{th}$  vision stage, and the channel dimension of linguistic features. The first token  $l_{cls}$  of linguistic expression features indicates a special [CLS] token, which is the global representation that understands the linguistic expression at the sentence level. The word token  $l_j$  indicates the local representation of  $j^{th}$  word. The advanced linguistic expression tokens  $\hat{E}_{\mathcal{L}}$  are extracted by the cross-attention layers using the vision features as key-value to improve the comprehension for the language contexts.

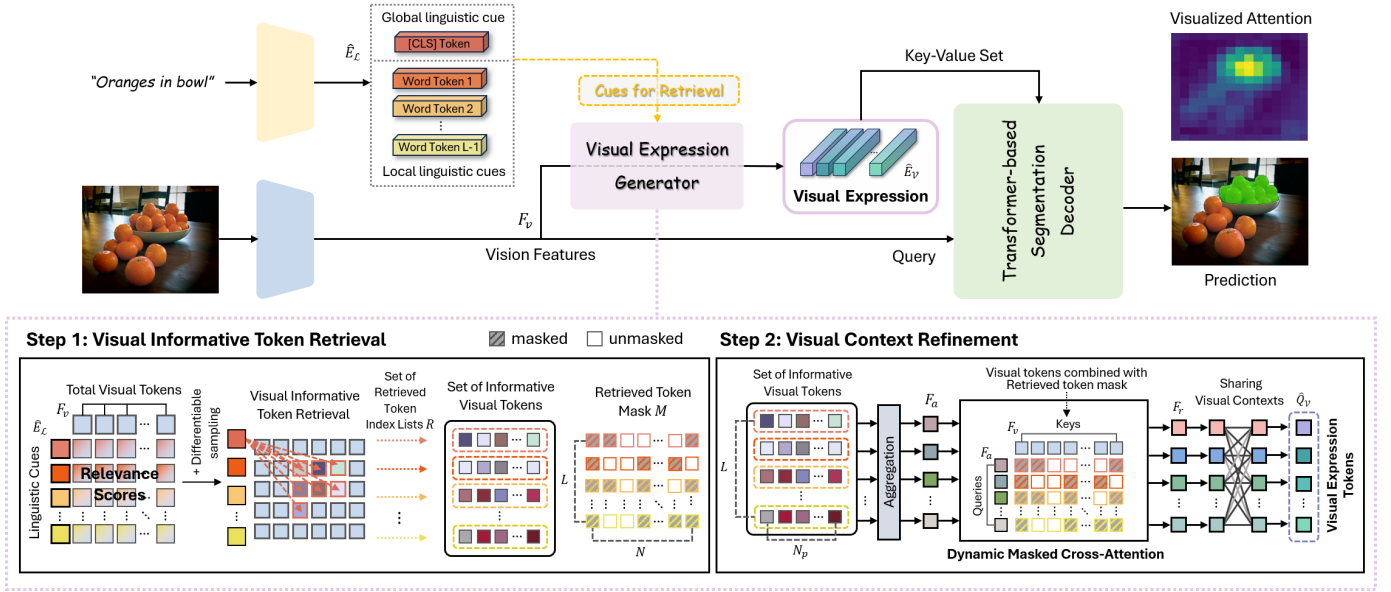


Fig. 2: Overview of Visual Informative Part Attention (VIPA) framework. VIPA robustly guides the network’s attention to the region of interest by exploiting the visual expression generated from the retrieved informative parts of visual contexts.

### B. Visual Expression Generator

To effectively guide the network to the region of interest, we produce the visual expression, which contains structural and semantic visual contexts. As shown in Fig. 2, the visual expression generator consists of the following two steps.

**Visual Informative Token Retrieval.** To retrieve the informative visual tokens, this step exploits local-global linguistic contexts as cues to consider both comprehensive context and attribute contexts. First, the vision features  $F_v (= F_4) \in \mathbb{R}^{N \times C}$  and the advanced local-global linguistic tokens  $\hat{E}_L$  are embedded into the joint embedding space by the linear projection  $\phi$ , where  $N$  is the total number of vision pixels. Then, the relevance score map  $S_c \in \mathbb{R}^{L \times N}$  between the vision tokens and the linguistic tokens is computed as:

$$X = \phi^V(F_v), Y = \phi^L(\hat{E}_L), S_c = \mathcal{C}(X, Y), \quad (1)$$

where  $\mathcal{C}$  denote the cosine similarity function. To retrieve the informative visual tokens based on the higher relevance scores per linguistic cue, we employ the differentiable sampling technique [45] during training, because the naive retrieval operation using the index list of the retrieved visual tokens is non-differentiable.

$$S' = \text{Softmax}((S_c + g)/\tau), R = \mathcal{R}(S', r), \quad (2)$$

$$M = \text{sampling}(R) \in \{0, 1\}^{L \times N}, \quad (3)$$

where  $g$  and  $\mathcal{R}$  denote a gumbel distribution and a relevance-based retrieval operation that retrieves the informative visual tokens based on the higher relevance scores per linguistic cue.  $\tau$  is a learnable parameter.  $r$  is a ratio of the retrieved tokens to total visual tokens.  $R \in \mathbb{R}^{L \times N_p}$  is the set of the retrieved informative visual token index lists per linguistic token, where  $N_p$  denotes the number of the retrieved visual tokens. The retrieved token mask  $M \in \mathbb{R}^{L \times N}$ , where ‘1’ indicates a informative token and ‘0’ is not in the region of interest, is

obtained based on the set  $R$  of the retrieved informative visual token index lists. The vision features  $F_v$  and the retrieved token mask  $M$  are passed to the next step.

To prevent the high relevance scores between the linguistic cues and the incorrect regions, the relevance score map  $s \in \mathbb{R}^{1 \times N}$  of the global linguistic token is supervised by a pixel contrastive loss:

$$\text{loss}_c = \begin{cases} -\log(\sigma(s_z)) & \text{if } z \in \mathcal{Z}^+ \\ -\log(1 - \sigma(s_z)) & \text{if } z \in \mathcal{Z}^- \end{cases}, \quad (4)$$

where  $\mathcal{Z}^+$  and  $\mathcal{Z}^-$  denote the set of the relevant pixels and irrelevant pixels for the ground truth target regions.  $\sigma$  is a sigmoid function. The pixel contrastive loss [4] encourages that the relevant pixels are embedded closer together for high relevance score and the irrelevant pixels are embedded far apart for low relevance score.

**Visual Context Refinement.** Rather than simply aggregating the retrieved information, we refine the informative visual tokens from the retrieved tokens to reduce the possibility of being distracted by noise information and to devote more attention to semantic information. In this step, the aggregated visual tokens  $F_a \in \mathbb{R}^{L \times D}$  corresponding to each linguistic cue are first obtained by the summation of the retrieved visual tokens and the linear projection. Then, the visual tokens  $F_r \in \mathbb{R}^{L \times D}$  are extracted by adaptively refining each aggregated visual token  $F_a$  via the dynamic masked cross-attention mechanism for mitigating noise information and devoting more attention to semantic information as:

$$F_a = \text{linear}(\sum_{N_p}^N (\text{repeat}(F_v, L) \odot M)) \in \mathbb{R}^{L \times D}, \quad (5)$$

$$\hat{F} = \text{MHCA}(F_a, F_v, M) + F_a, F_r = \text{MLP}(\hat{F}) + \hat{F}, \quad (6)$$

where  $\odot$  is element-wise multiplication, and  $\text{repeat}(f, x)$  indicates repeating the  $f$  feature  $x$  times to expand the shape.

TABLE I: Performance comparison with the state-of-the-art methods on four public referring image segmentation datasets. LLM-based models are marked in gray.  $\dagger$  indicates models trained on multiple RefCOCO series datasets with removed validation and testing images to prevent data leakage. For ReferIt dataset, only ReferIt training set is used.

| Method  | Publication | Vision Model | Language Model | RefCOCO      |              |              | RefCOCO+     |              |              | RefCOCOg     |              | ReferIt      |      |
|---|-------------|--------------|----------------|--------------|--------------|--------------|--------------|--------------|--------------|--------------|--------------|--------------|------|
|   |             |              |                | val          | test A       | test B       | val          | test A       | test B       | val          | test         | val          | test |
| <i>LLM-based RIS methods + additional vision-language training datasets</i> |             |              |                |              |              |              |              |              |              |              |              |              |      |
| LISA-7B [6]   | CVPR 2024   | SAM-H        | Vicuna-7B      | 74.9         | 79.1         | 72.3         | 65.1         | 70.8         | 58.1         | 67.9         | 70.6         | -            | -    |
| PixelLM [15]  | CVPR 2024   | CLIP-VIT-L   | Vicuna-7B      | 73.0         | 76.5         | 68.2         | 66.3         | 71.7         | 58.3         | 69.3         | 70.5         | -            | -    |
| GSVA-7B [16]  | CVPR 2024   | SAM-H        | Vicuna-7B      | 77.2         | 78.9         | 73.5         | 65.9         | 69.6         | 59.8         | 72.7         | 73.3         | -            | -    |
| GLaMM [17]  | CVPR 2024   | SAM-H        | Vicuna-7B      | 79.5         | 83.2         | 76.9         | 72.6         | 78.7         | 64.6         | 74.2         | 74.9         | -            | -    |
| SAM4MLLM-7B [46]  | ECCV 2024   | SAM-XL       | Qwen-VL-7B     | 76.2         | 80.1         | 72.0         | 71.2         | 75.9         | 64.3         | 74.2         | 74.3         | -            | -    |
| Text4Seg-7B [47]  | ICLR 2025   | SAM-H        | Vicuna-7B      | 79.3         | 81.9         | 76.2         | 72.1         | 77.6         | 66.1         | 72.1         | 73.9         | -            | -    |
| SegLLM [48]   | ICLR 2025   | SAM-H        | Vicuna-7B      | 80.2         | 81.5         | 75.4         | 70.3         | 73.0         | 62.5         | 72.6         | 73.6         | -            | -    |
| F-LMM [49]  | CVPR 2025   | SAM-L        | LLaMA2-7B      | 75.2         | -            | -            | 63.7         | -            | -            | 67.1         | -            | -            | -    |
| <i>Transformer-based RIS methods (oIoU)</i>                                 |             |              |                |              |              |              |              |              |              |              |              |              |      |
| VLT [7]   | TPAMI 2023  | Swin-B       | BERT-B         | 72.96        | 75.96        | 69.60        | 63.53        | 68.43        | 56.92        | 63.49        | 66.22        | -            | -    |
| ReLA [50]   | CVPR 2023   | Swin-B       | BERT-B         | 73.82        | 76.48        | 70.18        | 66.04        | 71.02        | 57.65        | 65.00        | 65.97        | -            | -    |
| DMMI [5]  | ICCV 2023   | Swin-B       | BERT-B         | 74.13        | 77.13        | 70.16        | 63.98        | 69.73        | 57.03        | 63.46        | 64.19        | -            | -    |
| LQMFormer [42]  | CVPR 2024   | Swin-B       | BERT-B         | 74.16        | 76.82        | 71.04        | 65.91        | 71.84        | 57.59        | 64.73        | 66.04        | -            | -    |
| CGFormer [29]   | CVPR 2023   | Swin-B       | BERT-B         | 74.75        | 77.30        | 70.64        | 64.54        | 71.00        | 57.14        | 64.68        | 65.09        | 73.36        | -    |
| MagNet [8]  | CVPR 2024   | Swin-B       | BERT-B         | 75.24        | 78.24        | 71.05        | 66.16        | 71.32        | 58.14        | 65.36        | 66.03        | -            | -    |
| <b>VIPA (Ours)</b>  | -           | Swin-B       | BERT-B         | <b>75.84</b> | <b>78.58</b> | <b>72.20</b> | <b>66.91</b> | <b>72.44</b> | <b>60.15</b> | <b>65.93</b> | <b>67.37</b> | <b>74.55</b> | -    |
| PolyFormer-B $\dagger$ [51]   | CVPR 2023   | Swin-B       | BERT-B         | 74.82        | 76.64        | 71.06        | 67.64        | 72.89        | 59.33        | 67.76        | 69.05        | 71.91        | -    |
| MagNet $\dagger$ [8]  | CVPR 2024   | Swin-B       | BERT-B         | 76.55        | 78.27        | 72.15        | 68.10        | 73.64        | 61.81        | 67.79        | 69.29        | -            | -    |
| <b>VIPA<math>\dagger</math> (Ours)</b>                                      | -           | Swin-B       | BERT-B         | <b>78.14</b> | <b>80.56</b> | <b>75.24</b> | <b>70.15</b> | <b>75.22</b> | <b>63.34</b> | <b>70.01</b> | <b>71.77</b> | <b>74.55</b> | -    |
| <i>Transformer-based RIS methods (mIoU)</i>                                 |             |              |                |              |              |              |              |              |              |              |              |              |      |
| CGFormer [29]   | CVPR 2023   | Swin-B       | BERT-B         | 76.93        | 78.70        | 73.32        | 68.56        | 73.76        | 61.72        | 67.57        | 67.83        | 66.42        | -    |
| DETRIS-B [52]   | AAAI 2025   | DINOv2-B     | CLIP           | 76.0         | 78.2         | 73.5         | 68.9         | 74.0         | 61.5         | 67.9         | 68.1         | -            | -    |
| <b>VIPA (Ours)</b>  | -           | Swin-B       | BERT-B         | <b>78.68</b> | <b>79.93</b> | <b>75.98</b> | <b>70.42</b> | <b>74.64</b> | <b>62.96</b> | <b>69.98</b> | <b>70.94</b> | <b>67.88</b> | -    |
| PolyFormer-B $\dagger$ [51]   | CVPR 2023   | Swin-B       | BERT-B         | 75.96        | 77.09        | 73.22        | 70.65        | 74.51        | 64.64        | 69.36        | 69.88        | 65.98        | -    |
| EEVG $\dagger$ [53]   | ECCV 2024   | ViT-B        | BERT-B         | 78.23        | 79.27        | 76.58        | 69.04        | 72.65        | 62.33        | 69.15        | 70.01        | -            | -    |
| <b>VIPA<math>\dagger</math> (Ours)</b>                                      | -           | Swin-B       | BERT-B         | <b>80.97</b> | <b>82.63</b> | <b>78.53</b> | <b>73.69</b> | <b>77.58</b> | <b>67.44</b> | <b>73.60</b> | <b>74.97</b> | <b>67.88</b> | -    |

$\text{MHCA}(q, kv, m)$  is the multi-head cross-attention using  $q$  as queries,  $kv$  as key-value pairs and  $m$  as masks. By using the retrieved token mask  $M$  corresponding to each linguistic cue in the masked cross-attention, the intermediate visual tokens  $\hat{F} \in \mathbb{R}^{L \times D}$  per linguistic cue can capture semantic information from the informative visual tokens retrieved by the corresponding linguistic cue.

The visual expression tokens  $\hat{E}_{\mathcal{V}} = [v_{cls}, v_1, \dots, v_{L-1}] \in \mathbb{R}^{L \times D}$  are finally produced by mutually sharing informative visual attributes to acquire visual contextual information as:

$$\hat{E} = \text{MHSA}(F_r) + F_r, \quad \hat{E}_{\mathcal{V}} = \text{MLP}(\hat{E}) + \hat{E}, \quad (7)$$

where MHSA and  $\hat{E}$  indicate the multi-head self-attention, and the intermediate features, respectively. In this way, the visual expression captures semantic visual contexts for the fine-grained target segmentation.

### C. Segmentation Decoder with Visual Informative Part Attention

The visual expression  $\hat{E}_{\mathcal{V}}$  generated from the retrieved informative visual tokens is used as a key-value set, which serves as the target information provider in the Transformer-based segmentation decoder. In particular, the visual expression provides key-value representations that are aligned with the visual feature space of the query. This minimizes modality gap between the query and key-value spaces than using language-based key-value representations. Thus, VIPA enhances semantic consistency in the attention mechanism.

At each stage of the segmentation decoder, the cross-attention layer, which uses vision features as a query and visual expression tokens as a key-value set, is employed to highlight the target regions, as follows:

$$F_o = \text{MHCA}(F_v, \hat{E}_{\mathcal{V}}) + F_v, \quad F_d = \text{MLP}(F_o) + F_o, \quad (8)$$

where  $\text{MHCA}(q, kv)$  denotes the multi-head cross-attention using  $q$  as a query,  $kv$  as a key-value set. The decoder can focus its attention on the fine-grained regions of interest thanks to the guidance by the informative parts of visual contexts. The vision decoder features  $F_d$  are then upsampled and concatenated with the corresponding vision encoder features to feed into the next decoder stage. The final segmentation map is projected to a binary class mask by a linear projection layer. The binary cross-entropy loss and the dice loss are used for the network training.

## IV. EXPERIMENTS

### A. Implementation Details

**Settings.** Our method was implemented in PyTorch [54]. The vision encoder is Swin-B [55] initialized with the pretrained weight on ImageNet-22K [56]. The language encoder is BERT-base [57] initialized with the official pretrained weight of the uncased version. The decoder was randomly initialized. We trained models for 40 epochs with 16 batch size on 24G RTX4090 GPUs. We used the AdamW [58] optimizer with initial learning rate of 3e-5 and adopted the polynomial

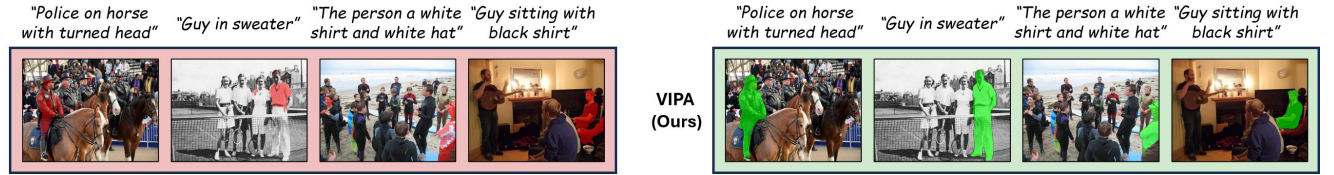


Fig. 3: Qualitative comparison with the LLM-based RIS model [6] on RefCOCO+.

TABLE II: Comparison of more recent transformer-based methods using BEiT3 [63] as encoder.

| Method             | Publication | RefCOCO      |              |              | RefCOCO+     |              |              | RefCOCOg     |              |
|--------------------|-------------|--------------|--------------|--------------|--------------|--------------|--------------|--------------|--------------|
|                    |             | val          | test A       | test B       | val          | test A       | test B       | val          | test         |
| C3VG [64]          | AAAI'25     | 81.37        | 82.93        | 79.12        | 77.05        | 79.61        | 72.40        | 76.34        | 77.10        |
| DeRIS-B [65]       | ICCV'25     | 81.99        | 82.97        | 80.14        | 75.62        | 79.16        | 71.63        | 76.30        | 77.15        |
| <b>VIPA (Ours)</b> | -           | <b>82.41</b> | <b>83.64</b> | <b>80.57</b> | <b>77.36</b> | <b>80.19</b> | <b>72.48</b> | <b>76.72</b> | <b>77.45</b> |

TABLE III: Computational comparison with recent methods on RefCOCOg *val*. Inference times are measured in Brain Floating Point 16 (BF16) for LLM-based models and Floating Point 32 (FP32) for Transformer-based models. LLM-based models are marked in gray.  $\ddagger$  indicates models trained with additional vision-language datasets.  $\dagger$  indicates models trained on multiple RefCOCO series datasets.

| Method                                 | GFLOPs | oIoU (%)     | Inference Time (ms) |
|--|--------|--------------|---------------------|
| GLaMM-7B $\ddagger$ [17]               | -      | 74.2         | 786 (BF16)          |
| LISA-7B $\ddagger$ [6]                 | 13,026 | 67.9         | 368 (BF16)          |
| <b>VIPA<math>\dagger</math> (Ours)</b> | 431    | <b>70.01</b> | 82 (FP32)           |
| DMMI [5]                               | 392    | 63.46        | 74 (FP32)           |
| CGFormer [29]                          | 950    | 64.68        | 105 (FP32)          |
| <b>VIPA (Ours)</b>                     | 431    | <b>65.93</b> | 82 (FP32)           |

learning rate decay scheduler. The input image resolution was  $480 \times 480$ . The maximum sequence length was set to 21 words including the [CLS] token for all datasets.

**Datasets.** RefCOCO [59], RefCOCO+ [59], RefCOCOg [60], [61] and ReferIt [62] are widely used datasets for referring image segmentation. RefCOCO contains 19,994 images with 142,209 language expressions for 50,000 objects, and RefCOCO+ contains 19,992 images with 141,564 expressions for 49,856 objects. The expressions in RefCOCO+ do not include words about absolute locations, which makes it more challenging than RefCOCO. RefCOCOg is the most challenging dataset, which has more complex and longer expressions. It contains 26,711 images with 104,560 language expressions for 54,822 objects. In addition, ReferIt contains 19,997 images with 130,364 language expression for 99,296 objects.

**Evaluation metrics.** Following prior works, we adopted the overall intersection-over-union (oIoU), mean intersection-over-union (mIoU), and precision at 0.5 and 0.7 thresholds. The oIoU is the ratio between the total intersection regions and the total union regions of all test samples. The mIoU is the average of IoUs between the predicted mask and the ground truth of all test samples. The precision is the percentage of test samples that have a IoU score higher than a threshold.

TABLE IV: Comparison for generalization setting using mIoU.

| Method             | RefCOCOg <i>val</i> |              | RefCOCOg <i>test</i> |              |
|--------------------|---------------------|--------------|----------------------|--------------|
|                    | seen                | unseen       | seen                 | unseen       |
| CRIS [4]           | 58.64               | 42.63        | 59.68                | 38.88        |
| LAVT [36]          | 60.16               | 42.33        | 60.37                | 41.38        |
| CGFormer [29]      | 65.60               | 46.11        | 65.67                | 42.31        |
| <b>VIPA (Ours)</b> | <b>66.52</b>        | <b>46.74</b> | <b>66.93</b>         | <b>43.06</b> |

### B. Comparison with Transformer-based RIS Methods

In Table I, we evaluated our approach with Transformer-based RIS methods on four benchmarks. Our method consistently showed strong performance on all splits of all datasets. In a single dataset setting, our VIPA outperformed the state-of-the-art methods on all dataset splits. In a multiple dataset setting, our method surpassed MagNet with remarkable improvements of 2.23% and 1.72% on average for RefCOCO and RefCOCO+, respectively. Especially, our VIPA showed considerable margins of 2.22% and 2.48% on each split of RefCOCOg, most challenging benchmark. For more comprehensive evaluation, we evaluated our method using mIoU. Compared to the state-of-the-art method CGFormer, our model significantly improved mIoU performance by 1.84% on average on four benchmarks.

In Table II, we experimented with the powerful encoder [63] for fair comparison with more recent methods. Our method showed competitive performance and can be successfully applied regardless of the specific encoder structure. Furthermore, in Table III, VIPA showed higher oIoU accuracy with comparable computations to DMMI and with 54.6% less GFLOPs than CGFormer on the most challenging dataset. These results demonstrate the effectiveness of our visual informative part attention framework.

In addition, we evaluated the generalizability of our framework compared to existing methods. In referring image segmentation, the ability to understand the visual context within the image is particularly crucial for achieving strong generalizability. In Table IV, we experimented with the generalization setting [29], where only the language descriptions for the seen target object classes are given during training and the model is not trained with the ground truth masks for the unseen target object classes. Under this setting, VIPA surpassed the existing methods and consistently showed performance improvements on both seen and unseen sets. These results suggest that our method achieves better generalization ability than previous RIS methods by learning semantic visual contexts via the visual expression.

TABLE V: Ablation for the effectiveness of the visual informative part attention framework. LE: Linguistic Expression tokens. VE: Visual Expression tokens (Ours). █ are ablation methods that leverage language-based tokens as key-value components in the segmentation decoder. Advanced LE indicates a method using visual-aware language tokens extracted by cross-attention with the vision features. █ is our method that leverages the visual expression, generated from the retrieved informative parts of visual contexts.

| Key-Value Set | RefCOCO+ val |              |              |              | RefCOCOg val |              |              |              |
|---------------|--------------|--------------|--------------|--------------|--------------|--------------|--------------|--------------|
|               | P@0.5        | P@0.7        | mIoU         | oIoU         | P@0.5        | P@0.7        | mIoU         | oIoU         |
| Vanilla LE    | 73.77        | 64.89        | 63.93        | 62.44        | 72.84        | 59.98        | 62.80        | 61.74        |
| Advanced LE   | 75.26        | 66.49        | 66.14        | 64.16        | 74.35        | 61.49        | 65.06        | 63.52        |
| VE            | <b>78.64</b> | <b>69.62</b> | <b>70.42</b> | <b>66.91</b> | <b>77.03</b> | <b>65.26</b> | <b>69.98</b> | <b>65.93</b> |

### C. Comparison with LLM-based RIS Methods

It is actually unfair to compare our model with LLM-based RIS models for the following reasons: (1) They adopt large-sized vision models and LLMs. (2) They use a strong segmentation model (SAM), which is trained with a large amount of segmentation datasets. (3) They are trained with large-scale vision-language grounding datasets. Despite the unfair comparison, we conducted comparison with LLM-based RIS models for further analysis. In Table III, our model showed competitive performance compared to LLM-based models by effectively providing structural and semantic visual contexts via the visual expression. In addition, our model showed significantly lower computations and was 5~10 times faster than LLM-based models. This result supports the importance of continuing to study transformer-based RIS methods in order to consider in terms of both performance and efficiency. Furthermore, we compared segmentation results in Fig. 3. Our model showed precise segmentation, whereas LISA segmented only some part of a target object or segment even non-target regions. These results indicate that our model has a stronger ability to guide the network’s attention to the fine-grained region of interest, compared to the LLM-based models.

### D. Ablation Studies

In ablation setting, our default model and ablation models are trained on each single dataset, not multiple datasets. For fair comparisons, all ablation models are based on our network and we added more layers into ablation models to maintain the model size similar to our default model.

**Effectiveness of Visual Expression.** In Table V, we conducted experiments to validate the effectiveness of exploiting the visual expression as the component of the key-value. We compared our method with two methods: ‘Vanilla LE’ method and ‘Advanced LE’ method. As a key-value set in the decoder, ‘Vanilla LE’ method uses the vanilla language encoder features, and ‘Advanced LE’ method uses the advanced language tokens extracted by cross-attention with the vision features. As shown in Table V, ‘Advanced LE’ method showed better performance than ‘Vanilla LE’ method on each dataset by improving the cross-modal alignment.

Different from these two ablation methods, our method uses the visual expression generated from the retrieved infor-

TABLE VI: Ablation studies for the design of the visual expression generator module. Our default design is marked in █.

|     | Design |        | RefCOCO+ val |              | RefCOCOg val |              |
|-----|--------|--------|--------------|--------------|--------------|--------------|
|     | Step 1 | Step 2 | mIoU         | oIoU         | mIoU         | oIoU         |
| (a) | ✗      | ✓      | 66.67        | 64.72        | 66.31        | 64.04        |
|     | ✓      | ✗      | 66.29        | 64.54        | 65.82        | 63.79        |
|     | ✓      | ✓      | <b>70.42</b> | <b>66.91</b> | <b>69.98</b> | <b>65.93</b> |
| (b) | Global | Local  | mIoU         | oIoU         | mIoU         | oIoU         |
|     | ✗      | ✗      | 66.67        | 64.72        | 66.31        | 64.04        |
|     | ✓      | ✗      | 67.64        | 65.15        | 67.60        | 64.79        |
|     | ✗      | ✓      | 68.05        | 65.27        | 67.33        | 64.75        |
|     | ✓      | ✓      | <b>70.42</b> | <b>66.91</b> | <b>69.98</b> | <b>65.93</b> |

mative visual tokens. Compared to these ablation methods, our VE method showed remarkable gains by 4.19% and 2.41% oIoU on RefCOCOg, the most challenging dataset. From an attention alignment perspective, these gains suggest that our approach minimizes the modality gap between the query and key-value spaces, enhancing semantic consistency in attention. These results also indicate that leveraging the visual expression as a key-value set provides the vision query features with semantic structural contexts of the informative regions more effectively, rather than projecting visual information into linguistic tokens (*i.e.*, advanced LE methods). Therefore, considering the informative parts of visual contexts in the attention mechanism of the segmentation decoder can improve the capability to guide the network towards the fine-grained region of interest on the referring segmentation task by enhancing attention coherence.

**Analysis on Design of Visual Expression Generator.** In Table VI (a), the removal of Step 1 (*i.e.*, visual informative token retrieval) resulted in significant drops. This indicates that leveraging the retrieved informative parts of visual tokens is effective in guiding the network to the target region compared to using the total visual tokens, as most visual pixel tokens in the image are not in the region of interest. The removal of Step 2 (*i.e.*, visual context refinement) also resulted in notable performance degradation. This step enables the visual expression to capture the semantic visual contexts by mitigating the noise information and considering the visual relationship between each informative visual token. Therefore, these ablation results demonstrate that each step of our module is necessary to generate the informative visual expression.

In Table VI (b), removing the use of the local linguistic cues showed performance drops compared to our full model. Removing the use of the global linguistic cue also decreased performance. Additionally, removing the use of both local-global linguistic cues, which exploits all vision tokens without the retrieval step, showed substantial drops in oIoU and mIoU. These results indicate that exploiting the linguistic context-relevant parts of visual contexts as a key-value set helps to effectively complement the limited target information of language inputs on referring image segmentation. Furthermore, leveraging both global and local linguistic cues allows the visual expression tokens to consider both the comprehensive context and the attribute contexts for the enriched visual contexts of fine-grained target regions.

**Encoder-type Agnostic.** We experimented with different en-

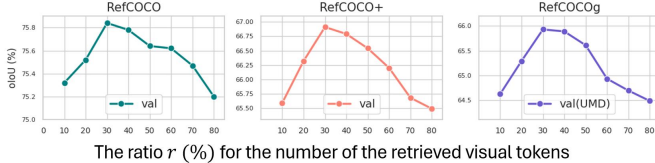
(a) Performance by increasing the value of  $r$ 

Fig. 4: Ablation study on the number of the retrieved informative visual tokens.

(b) Segmentation results at different  $r$ 

TABLE VII: Ablation for different encoder fusion types.

| Encoder Feature Extraction | Method | RefCOCO+     |              |              |
|----------------------------|--------|--------------|--------------|--------------|
|                            |        | val          | test A       | test B       |
| w/o Fusion                 | w/o VE | 62.74        | 68.41        | 55.82        |
|                            | w/ VE  | <b>65.15</b> | <b>71.17</b> | <b>58.34</b> |
| Late Fusion                | w/o VE | 63.88        | 69.65        | 57.07        |
|                            | w/ VE  | <b>66.74</b> | <b>72.21</b> | <b>59.73</b> |
| Early Fusion               | w/o VE | 64.16        | 69.86        | 57.39        |
|                            | w/ VE  | <b>66.91</b> | <b>72.44</b> | <b>60.15</b> |

TABLE VIII: Additional ablation on supervision by the contrastive loss. Our default design is marked in  .

| Method                   | RefCOCO+ val | RefCOCO+ test A | RefCOCO+ test B |
|--------------------------|--------------|-----------------|-----------------|
| w/o Supervision          | 65.93        | 71.50           | 59.26           |
| Direct thresholding loss | 66.52        | 71.93           | 59.60           |
| Pixel contrastive loss   | <b>66.91</b> | <b>72.44</b>    | <b>60.15</b>    |

coder types in Table VII to verify the versatility of our method and to analyze the impact of vision-language encoder alignment. Our method with early fusion showed higher performance than other types. Notably, across all encoder types, the introduction of visual expression consistently improves performance, including the setting without any explicit fusion in the encoder. This result demonstrates that our visual expression approach does not rely on a specific encoder design and can functions as an effective and complementary component regardless of the fusion strategy. Therefore, VIPA is encoder-type agnostic and can robustly enhance segmentation performance across diverse architectural choices.

**Number of Retrieved Tokens.** We analyzed the ratio  $r$  for the number of the retrieved visual tokens. Compared to the  $r$  values of 10 and 80, the  $r$  of 30 showed higher oIoU in Fig. 4 (a). In Fig. 4 (b), the  $r$  of 30 segmented more clearly, while the  $r$  of 10 missed some part of the target regions and the  $r$  of 80 even segmented other object regions. The smaller number of  $r$  resulted in a lack of information, where the informative visual tokens cannot be sufficiently exploited. In contrast, the larger number of  $r$  resulted in higher proportion of noise information and distracting the informativeness of the visual expression. Thus, the optimal  $r$  can exploit semantic visual information and filter out noise components to improve the robustness of the guidance capacity.

**Ablation for Supervision by Contrastive Loss.** In Table VIII, we experimented on supervising the relevance score map by the pixel contrastive loss. The contrastive loss is more effective to monitor the retrieval of informative visual tokens, compared to the direct thresholding loss. In addition, the contrastive loss helps to monitor the curation of the informative tokens

TABLE IX: Ablation study on the use of the article tokens at the process of retrieving informative visual contexts. Our default design is marked in  .

| Method       | RefCOCO val  |              | RefCOCO+ val |              | RefCOCOg val |              |
|--------------|--------------|--------------|--------------|--------------|--------------|--------------|
|              | mIoU         | oIoU         | mIoU         | oIoU         | mIoU         | oIoU         |
| w/o articles | 77.80        | 75.11        | 69.35        | 66.32        | 67.74        | 64.99        |
| All words    | <b>78.68</b> | <b>75.84</b> | <b>70.42</b> | <b>66.91</b> | <b>69.98</b> | <b>65.93</b> |

associated with the correct target region and to prevent the high relevance scores between the linguistic features and incorrect regions.

**Ablation for Using Article of Language.** we experimented the ablation on the use of the article tokens such as “the”, “a” and “an”, which are meaningless words in the input sentence, in the process of the visual informative token retrieval. As shown in Table IX, compared to using all word tokens, ‘w/o article’ resulted in 0.73%, 0.59% and 0.94% drops in oIoU on each dataset, respectively. These results indicate that the article tokens do not carry the noise information, and using all word tokens as linguistic cues are more effective at collecting the informative visual tokens. Since the relations of each word are considered during encoding the language input to capture the contextual information for the target object description, each language token is encoded with semantic representations.

### E. Qualitative Results

**t-SNE Visualizations.** In Fig. 5, we presented t-SNE visualizations and qualitative comparisons between our visual expression method and the ablated method that employs advanced language expression. The t-SNE exhibits the distribution of pixel tokens and visual and linguistic expression tokens in the embedding space. As shown in the t-SNE results, visual expression embeddings are closer to the target pixels, whereas the linguistic expression embeddings of the ablated model exhibit weaker alignment with target pixel embeddings.

Consistent with these observations, the qualitative results further demonstrate the advantage of visual expression. The ablated model either segmented only partial target regions (top row) or incorrectly attended to non-target regions (bottom row). In contrast, our method produces more accurate and complete segmentations by effectively incorporating semantically informative visual contexts. These results indicate that our visual informative part attention approach enhances semantic consistency in attention, leading to more robust segmentation performance.

**Visual Comparisons with Ablation Method.** We compared with the ablation method (*i.e.*, advanced language expression)

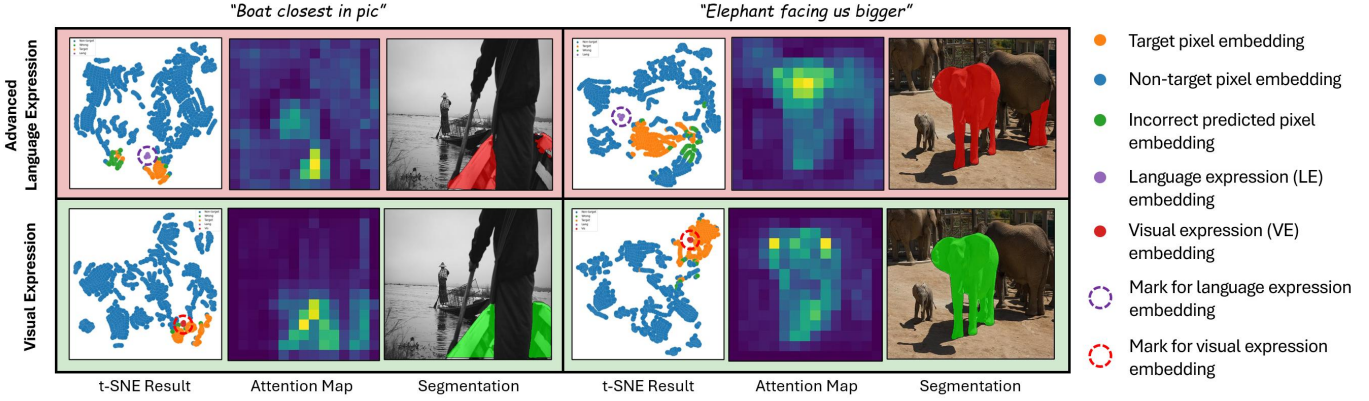


Fig. 5: t-SNE visualizations and qualitative comparisons between the ablation method (*i.e.*, advanced language expression) and our method (*i.e.*, visual expression).

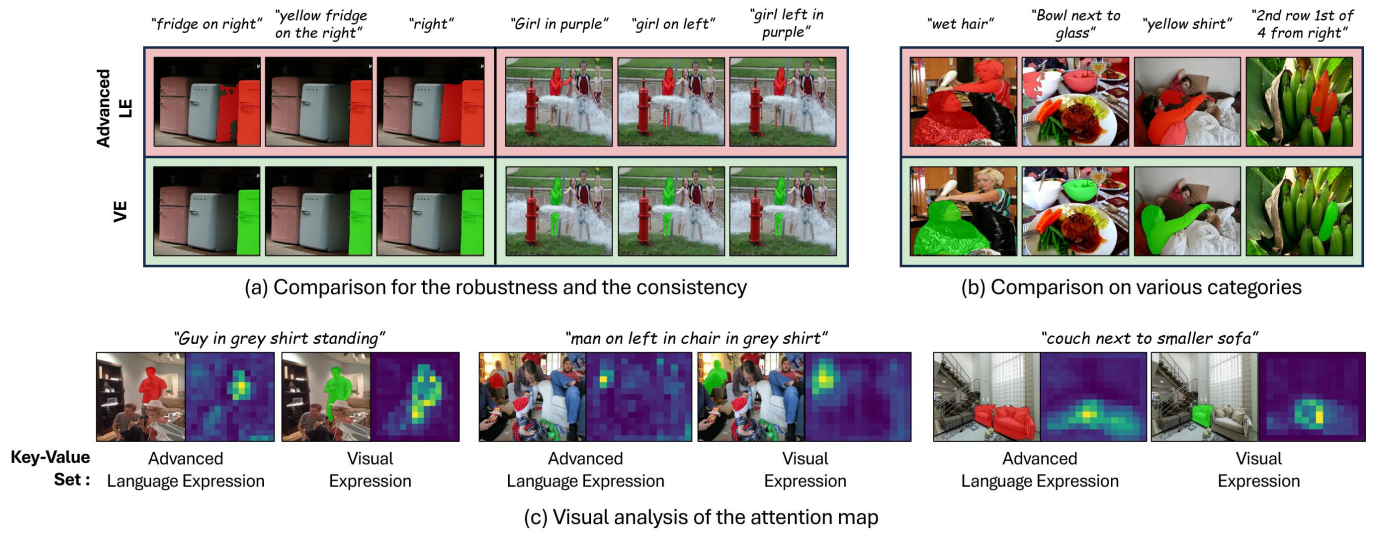


Fig. 6: (a-b) Visualized comparison with the ablation method (*i.e.*, advanced Language Expression (LE)) and our method (*i.e.*, Visual Expression (VE)). (c) Visual analysis of the attention map between vision query features and visual expression key-value set, and the attention map between vision query features and advanced language expression key-value set.

on different language expressions describing the same target object and on various target object categories in Fig. 6 (a) and (b), respectively. The ablation method inconsistently predicted the target regions and showed incorrect segmentation. In contrast, our VE method consistently predicted accurate regions for both large target regions and small target regions. These results indicate that our method enhances the adaptability to diverse language and image inputs.

**Visual analysis of Attention maps.** We presented additional visual analysis of the attention maps in Fig. 6 (c): one between the vision query (Q) features and the key-value (KV) set of the visual expression, and another between the vision query (Q) features and the key-value (KV) set of the advanced language expression. The visual expression robustly guides the network’s attention to the regions of interest, whereas the language expression fails to focus on the real target regions or highlights even wide non-target regions. These qualitative results support that our VIPA approach theoretically improves attention coherence and semantic consistency.

Concretely, the informative parts of the visual contexts, *visual expression*, provide KV representations that are aligned in the visual feature space of the query Q, yielding lower modality projection entropy than the language-based KVs. Therefore, this visual analysis demonstrates that our approach more effectively exploits the structural information for fine-grained segmentation, compared to the existing approach using visual-aware linguistic tokens.

**Qualitative Comparisons with Transformer-based RIS methods.** In Fig. 7 (a), we compared with previous methods using the advanced linguistic tokens as a key-value set. Ours segmented more clearly, whereas others incorrectly predicted and uncertainly segmented the regions. These indicate that our approach is more effective in improving visual understanding of the fine-grained target regions. In Fig. 7 (b), we visualized our results on longer and complex language inputs with the complicated images. These results indicate that VIPA is robust in challenging scenarios. All of these visual comparisons demonstrate that the visual expression can effectively serve as



Fig. 7: (a) Qualitative comparison with Transformer-based RIS methods. (b) Our results on long and difficult language inputs.

an advanced information provider in the attention mechanism of referring image segmentation. More various qualitative comparisons are provided in supplementary materials.

## V. CONCLUSION

We propose a novel Visual Informative Part Attention (VIPA) framework to more effectively exploit visual contexts for referring image segmentation. Our VIPA is the first study to leverage *visual expression*, generated from the informative parts of visual contexts, as a key-value set for the vision query feature in the attention mechanism of the referring segmentation decoder. The visual expression provides the key-value representations that are aligned in the visual feature space of the query. From an attention alignment standpoint, this design aligns the query and the key-value set within the visual modality space, reducing high-variance cross-modal projection and enhancing semantic consistency. Therefore, our approach robustly guides the network's attention to fine-grained target regions by providing structural and semantic visual information. Extensive comparisons and ablations demonstrate the effectiveness of exploiting retrieved informative visual parts for Transformer-based referring image segmentation.

## REFERENCES

- [1] S. Liu, T. Hui, S. Huang, Y. Wei, B. Li, and G. Li, "Cross-modal progressive comprehension for referring segmentation," *IEEE Transactions on Pattern Analysis and Machine Intelligence*, vol. 44, no. 9, pp. 4761–4775, 2021.
- [2] R. Hu, M. Rohrbach, and T. Darrell, "Segmentation from natural language expressions," in *Computer Vision–ECCV 2016: 14th European Conference, Amsterdam, The Netherlands, October 11–14, 2016, Proceedings, Part I 14*. Springer, 2016, pp. 108–124.
- [3] C. Liu, Z. Lin, X. Shen, J. Yang, X. Lu, and A. Yuille, "Recurrent multimodal interaction for referring image segmentation," in *Proceedings of the IEEE international conference on computer vision*, 2017, pp. 1271–1280.
- [4] Z. Wang, Y. Lu, Q. Li, X. Tao, Y. Guo, M. Gong, and T. Liu, "Cris: Clip-driven referring image segmentation," in *Proceedings of the IEEE/CVF conference on computer vision and pattern recognition*, 2022, pp. 11 686–11 695.
- [5] Y. Hu, Q. Wang, W. Shao, E. Xie, Z. Li, J. Han, and P. Luo, "Beyond one-to-one: rethinking the referring image segmentation," in *2023 IEEE/CVF International Conference on Computer Vision (ICCV) Proceedings*. Institute of Electrical and Electronics Engineers (IEEE), 2023.
- [6] X. Lai, Z. Tian, Y. Chen, Y. Li, Y. Yuan, S. Liu, and J. Jia, "Lisa: Reasoning segmentation via large language model," in *Proceedings of the IEEE/CVF Conference on Computer Vision and Pattern Recognition*, 2024, pp. 9579–9589.
- [7] H. Ding, C. Liu, S. Wang, and X. Jiang, "Vlt: Vision-language transformer and query generation for referring segmentation," *IEEE Transactions on Pattern Analysis and Machine Intelligence*, 2022.
- [8] Y. X. Chng, H. Zheng, Y. Han, X. Qiu, and G. Huang, "Mask grounding for referring image segmentation," in *Proceedings of the IEEE/CVF Conference on Computer Vision and Pattern Recognition*, 2024, pp. 26 573–26 583.
- [9] J. Wu, X. Li, X. Li, H. Ding, Y. Tong, and D. Tao, "Toward robust referring image segmentation," *IEEE Transactions on Image Processing*, vol. 33, pp. 1782–1794, 2024.
- [10] W. Li, Z. Zhao, H. Bai, and F. Su, "Bring adaptive binding prototypes to generalized referring expression segmentation," *IEEE Transactions on Multimedia*, 2025.
- [11] M. Xu, T. Xiao, Y. Liu, H. Tang, Y. Hu, and L. Nie, "Cmirnet: Cross-modal interactive reasoning network for referring image segmentation," *IEEE Transactions on Circuits and Systems for Video Technology*, 2024.
- [12] C. Shang, H. Li, H. Qiu, Q. Wu, F. Meng, T. Zhao, and K. N. Ngan, "Cross-modal recurrent semantic comprehension for referring image segmentation," *IEEE Transactions on Circuits and Systems for Video Technology*, vol. 33, no. 7, pp. 3229–3242, 2022.
- [13] C. Xiao, Q. Cao, Y. Zhong, X. Zhang, T. Wang, C. Yang, and L. Lan, "Temporal-enhanced multimodal transformer for referring multi-object tracking and segmentation," *IEEE Transactions on Circuits and Systems for Video Technology*, 2025.
- [14] H. Ding, S. Zhang, Q. Wu, S. Yu, J. Hu, L. Cao, and R. Ji, "Bilateral knowledge interaction network for referring image segmentation," *IEEE Transactions on Multimedia*, vol. 26, pp. 2966–2977, 2023.
- [15] Z. Ren, Z. Huang, Y. Wei, Y. Zhao, D. Fu, J. Feng, and X. Jin, "Pixelmm: Pixel reasoning with large multimodal model," in *Proceedings of the IEEE/CVF Conference on Computer Vision and Pattern Recognition*, 2024, pp. 26 374–26 383.
- [16] Z. Xia, D. Han, Y. Han, X. Pan, S. Song, and G. Huang, "Gsva: Generalized segmentation via multimodal large language models," in *Proceedings of the IEEE/CVF Conference on Computer Vision and Pattern Recognition*, 2024, pp. 3858–3869.
- [17] H. Rasheed, M. Maaz, S. Shaji, A. Shaker, S. Khan, H. Cholakkal, R. M. Anwer, E. Xing, M.-H. Yang, and F. S. Khan, "Glaam: Pixel grounding large multimodal model," in *Proceedings of the IEEE/CVF Conference on Computer Vision and Pattern Recognition*, 2024, pp. 13 009–13 018.

[18] H. Touvron, L. Martin, K. Stone, P. Albert, A. Almahairi, Y. Babaei, N. Bashlykov, S. Batra, P. Bhargava, S. Bhosale *et al.*, “Llama 2: Open foundation and fine-tuned chat models,” *arXiv preprint arXiv:2307.09288*, 2023.

[19] W.-L. Chiang, Z. Li, Z. Lin, Y. Sheng, Z. Wu, H. Zhang, L. Zheng, S. Zhuang, Y. Zhuang, J. E. Gonzalez *et al.*, “Vicuna: An open-source chatbot impressing gpt-4 with 90%\* chatgpt quality,” *See https://vicuna.lmsys.org (accessed 14 April 2023)*, vol. 2, no. 3, p. 6, 2023.

[20] Z. Xu, Z. Chen, Y. Zhang, Y. Song, X. Wan, and G. Li, “Bridging vision and language encoders: Parameter-efficient tuning for referring image segmentation,” in *Proceedings of the IEEE/CVF International Conference on Computer Vision*, 2023, pp. 17 503–17 512.

[21] S. Yu, P. H. Seo, and J. Son, “Zero-shot referring image segmentation with global-local context features,” in *Proceedings of the IEEE/CVF conference on computer vision and pattern recognition*, 2023, pp. 19 456–19 465.

[22] H. Ding, X. Jiang, B. Shuai, A. Q. Liu, and G. Wang, “Semantic segmentation with context encoding and multi-path decoding,” *IEEE Transactions on Image Processing*, vol. 29, pp. 3520–3533, 2020.

[23] B. Shuai, H. Ding, T. Liu, G. Wang, and X. Jiang, “Toward achieving robust low-level and high-level scene parsing,” *IEEE Transactions on Image Processing*, vol. 28, no. 3, pp. 1378–1390, 2018.

[24] J.-h. Shim, H. Yu, K. Kong, and S.-J. Kang, “Feedformer: revisiting transformer decoder for efficient semantic segmentation,” in *Proceedings of the AAAI Conference on Artificial Intelligence*, vol. 37, 2023, pp. 2263–2271.

[25] B. Kang, S. Moon, Y. Cho, H. Yu, and S.-J. Kang, “Metaseg: Metaformer-based global contexts-aware network for efficient semantic segmentation,” in *Proceedings of the IEEE/CVF Winter Conference on Applications of Computer Vision (WACV)*, January 2024, pp. 434–443.

[26] H. Yu, Y. Cho, B. Kang, S. Moon, K. Kong, and S.-J. Kang, “Embedding-free transformer with inference spatial reduction for efficient semantic segmentation,” in *European Conference on Computer Vision*. Springer, 2024, pp. 92–110.

[27] N. Ravi, V. Gabeur, Y.-T. Hu, R. Hu, C. Ryali, T. Ma, H. Khedr, R. Rädle, C. Rolland, L. Gustafson *et al.*, “Sam 2: Segment anything in images and videos,” *arXiv preprint arXiv:2408.00714*, 2024.

[28] Y. Cho, H. Yu, and S.-J. Kang, “Cross-aware early fusion with stage-divided vision and language transformer encoders for referring image segmentation,” *IEEE Transactions on Multimedia*, vol. 26, pp. 5823–5833, 2023.

[29] J. Tang, G. Zheng, C. Shi, and S. Yang, “Contrastive grouping with transformer for referring image segmentation,” in *Proceedings of the IEEE/CVF Conference on Computer Vision and Pattern Recognition*, 2023, pp. 23 570–23 580.

[30] R. Li, K. Li, Y.-C. Kuo, M. Shu, X. Qi, X. Shen, and J. Jia, “Referring image segmentation via recurrent refinement networks,” in *Proceedings of the IEEE Conference on Computer Vision and Pattern Recognition*, 2018, pp. 5745–5753.

[31] G. Hua, M. Liao, S. Tian, Y. Zhang, and W. Zou, “Multiple relational learning network for joint referring expression comprehension and segmentation,” *IEEE Transactions on Multimedia*, vol. 25, pp. 8805–8816, 2023.

[32] L. Ye, M. Rochan, Z. Liu, and Y. Wang, “Cross-modal self-attention network for referring image segmentation,” in *Proceedings of the IEEE/CVF conference on computer vision and pattern recognition*, 2019, pp. 10 502–10 511.

[33] C. Zhu, Y. Zhou, Y. Shen, G. Luo, X. Pan, M. Lin, C. Chen, L. Cao, X. Sun, and R. Ji, “Seqtr: A simple yet universal network for visual grounding,” in *Computer Vision–ECCV 2022: 17th European Conference, Tel Aviv, Israel, October 23–27, 2022, Proceedings, Part XXXV*. Springer, 2022, pp. 598–615.

[34] N. Kim, D. Kim, C. Lan, W. Zeng, and S. Kwak, “Restr: Convolution-free referring image segmentation using transformers,” in *Proceedings of the IEEE/CVF Conference on Computer Vision and Pattern Recognition*, 2022, pp. 18 145–18 154.

[35] C. Liu, X. Jiang, and H. Ding, “Instance-specific feature propagation for referring segmentation,” *IEEE Transactions on Multimedia*, vol. 25, pp. 3657–3667, 2022.

[36] Z. Yang, J. Wang, Y. Tang, K. Chen, H. Zhao, and P. H. Torr, “Lavt: Language-aware vision transformer for referring image segmentation,” in *Proceedings of the IEEE/CVF Conference on Computer Vision and Pattern Recognition*, 2022, pp. 18 155–18 165.

[37] H. Ding and et al., “Vlt: Vision-language transformer and query generation for referring segmentation,” *TPAMI*, 2022.

[38] W. Li, C. Pang, W. Nie, H. Tian, and A.-A. Liu, “Bidirectional mask selection for zero-shot referring image segmentation,” *IEEE Transactions on Circuits and Systems for Video Technology*, 2024.

[39] X. Wang, S. Zhang, S. Li, K. Li, K. Kallidromitis, Y. Kato, K. Kozuka, and T. Darrell, “Segllm: Multi-round reasoning segmentation with large language models,” in *The Thirteenth International Conference on Learning Representations*, 2025.

[40] S. Yang, T. Qu, X. Lai, Z. Tian, B. Peng, S. Liu, and J. Jia, “Lisa++: An improved baseline for reasoning segmentation with large language model,” *arXiv preprint arXiv:2312.17240*, 2023.

[41] S.-A. Liu, H. Xie, J. Ge, and Y. Zhang, “Refersam: Unleashing segment anything model for referring image segmentation,” *IEEE Transactions on Circuits and Systems for Video Technology*, 2025.

[42] N. A. Shah, V. VS, and V. M. Patel, “Lqmformer: Language-aware query mask transformer for referring image segmentation,” in *Proceedings of the IEEE/CVF Conference on Computer Vision and Pattern Recognition*, 2024, pp. 12 903–12 913.

[43] Y. Wang, J. Li, X. Zhang, B. Shi, C. Li, W. Dai, H. Xiong, and Q. Tian, “Barleria: An efficient tuning framework for referring image segmentation,” in *The Twelfth International Conference on Learning Representations*, 2024.

[44] C. Liu, H. Ding, Y. Zhang, and X. Jiang, “Multi-modal mutual attention and iterative interaction for referring image segmentation,” *IEEE Transactions on Image Processing*, vol. 32, pp. 3054–3065, 2023.

[45] E. Jang, S. Gu, and B. Poole, “Categorical reparameterization with gumbel-softmax,” *arXiv preprint arXiv:1611.01144*, 2016.

[46] Y.-C. Chen, W.-H. Li, C. Sun, Y.-C. F. Wang, and C.-S. Chen, “Sam4mllm: Enhance multi-modal large language model for referring expression segmentation,” in *European Conference on Computer Vision*. Springer, 2025, pp. 323–340.

[47] M. Lan, C. Chen, Y. Zhou, J. Xu, Y. Ke, X. Wang, L. Feng, and W. Zhang, “Text4seg: Reimagining image segmentation as text generation,” *arXiv preprint arXiv:2410.09855*, 2024.

[48] X. Wang, S. Zhang, S. Li, K. Li, K. Kallidromitis, Y. Kato, K. Kozuka, and T. Darrell, “Segllm: Multi-round reasoning segmentation with large language model,” in *The Thirteenth International Conference on Learning Representations*, 2024.

[49] S. Wu, S. Jin, W. Zhang, L. Xu, W. Liu, W. Li, and C. C. Loy, “F-lmm: Grounding frozen large multimodal models,” *arXiv preprint arXiv:2406.05821*, 2024.

[50] C. Liu, H. Ding, and X. Jiang, “Gres: Generalized referring expression segmentation,” in *Proceedings of the IEEE/CVF Conference on Computer Vision and Pattern Recognition*, 2023, pp. 23 592–23 601.

[51] J. Liu, H. Ding, Z. Cai, Y. Zhang, R. K. Satzoda, V. Mahadevan, and R. Manmatha, “Polyformer: Referring image segmentation as sequential polygon generation,” in *Proceedings of the IEEE/CVF Conference on Computer Vision and Pattern Recognition*, 2023, pp. 18 653–18 663.

[52] J. Huang, Z. Xu, T. Liu, Y. Liu, H. Han, K. Yuan, and X. Li, “Densely connected parameter-efficient tuning for referring image segmentation,” *arXiv preprint arXiv:2501.08580*, 2025.

[53] W. Chen, L. Chen, and Y. Wu, “An efficient and effective transformer decoder-based framework for multi-task visual grounding,” *arXiv preprint arXiv:2408.01120*, 2024.

[54] A. Paszke, S. Gross, F. Massa, A. Lerer, J. Bradbury, G. Chanan, T. Killeen, Z. Lin, N. Gimelshein, L. Antiga *et al.*, “Pytorch: An imperative style, high-performance deep learning library,” *Advances in neural information processing systems*, vol. 32, 2019.

[55] Z. Liu, Y. Lin, Y. Cao, H. Hu, Y. Wei, Z. Zhang, S. Lin, and B. Guo, “Swin transformer: Hierarchical vision transformer using shifted windows,” in *Proceedings of the IEEE/CVF International Conference on Computer Vision*, 2021, pp. 10 012–10 022.

[56] A. Krizhevsky, I. Sutskever, and G. E. Hinton, “Imagenet classification with deep convolutional neural networks,” *Advances in neural information processing systems*, vol. 25, 2012.

[57] J. Devlin, M.-W. Chang, K. Lee, and K. Toutanova, “Bert: Pre-training of deep bidirectional transformers for language understanding,” *arXiv preprint arXiv:1810.04805*, 2018.

[58] I. Loshchilov and F. Hutter, “Decoupled weight decay regularization,” *arXiv preprint arXiv:1711.05101*, 2017.

[59] L. Yu, P. Poirson, S. Yang, A. C. Berg, and T. L. Berg, “Modeling context in referring expressions,” in *European Conference on Computer Vision*. Springer, 2016, pp. 69–85.

[60] J. Mao, J. Huang, A. Toshev, O. Camburu, A. L. Yuille, and K. Murphy, “Generation and comprehension of unambiguous object descriptions,” in *Proceedings of the IEEE conference on computer vision and pattern recognition*, 2016, pp. 11–20.

- [61] V. K. Nagaraja, V. I. Morariu, and L. S. Davis, “Modeling context between objects for referring expression understanding,” in *Computer Vision–ECCV 2016: 14th European Conference, Amsterdam, The Netherlands, October 11–14, 2016, Proceedings, Part IV 14*. Springer, 2016, pp. 792–807.
- [62] S. Kazemzadeh, V. Ordonez, M. Matten, and T. Berg, “Referitgame: Referring to objects in photographs of natural scenes,” in *Proceedings of the 2014 conference on empirical methods in natural language processing (EMNLP)*, 2014, pp. 787–798.
- [63] W. Wang, H. Bao, L. Dong, J. Bjorck, Z. Peng, Q. Liu, K. Aggarwal, O. K. Mohammed, S. Singhal, S. Som *et al.*, “Image as a foreign language: Beit pretraining for vision and vision-language tasks,” in *Proceedings of the IEEE/CVF Conference on Computer Vision and Pattern Recognition*, 2023, pp. 19 175–19 186.
- [64] M. Dai, J. Li, J. Zhuang, X. Zhang, and W. Yang, “Multi-task visual grounding with coarse-to-fine consistency constraints,” in *Proceedings of the AAAI Conference on Artificial Intelligence*, vol. 39, no. 3, 2025, pp. 2618–2626.
- [65] M. Dai, W. Cheng, J.-j. Liu, S. Yang, W. Cai, Y. Sun, and W. Yang, “Deris: Decoupling perception and cognition for enhanced referring image segmentation through loopback synergy,” *arXiv preprint arXiv:2507.01738*, 2025.



**Yubin Cho** received the B.S. degree with double major in Mechanical Engineering and Artificial Intelligence from Sogang University, South Korea, in 2022, and the M.S. degree with the School of Artificial Intelligence, Sogang University, in 2024. She is currently with the AI Lab of CTO division, LG Electronics. Her current research interests include computer vision, multi-modal learning and embodied AI.



**Hyunwoo Yu** received the B.S. degree in Physics from Kangwon University, South Korea, in 2021. He is currently working toward the Ph.D. degree with the School of Electronic Engineering, Sogang University, South Korea. His current research interests include computer vision, multi-modal learning and pixel-level scene understanding.



**Kyeongbo Kong** received the B.S. degree in electronics engineering from Sogang University, Seoul, South Korea, in 2015, and the M.S. and Ph.D. degrees in electrical engineering from the Pohang University of Science and Technology (POSTECH), Pohang, South Korea, in 2017 and 2020, respectively. From 2020 to 2021, he was worked as a Postdoctoral Fellow with the Department of Electrical Engineering, POSTECH, Pohang, South Korea. From 2021 to 2023, he was an Assistant Professor of Media School at Pukyong National University, Busan. He is currently an Associate Professor of Electrical and Electronics Engineering at Pusan National University. His current research interests include image processing, computer vision, machine learning, and deep learning.



**Kyomin Sohn** is a Samsung Master (VP of Technology) in Samsung Electronics and he is responsible for future architecture and circuit technology of DRAM. He received the B.S. and M.S. degrees in Electrical Engineering in 1994 and 1996, respectively, from Yonsei University, Seoul. From 1996 to 2003, he was with Samsung Electronics, Korea, involved in SRAM Design Team. He designed various kinds of high-speed SRAMs. He received the Ph.D. degree in EECS in 2007 from KAIST, Korea. He rejoined Samsung Electronics in 2007, where he has been involved in DRAM Design Team. He led the development of HBM2 DRAMs and HBM-PIM. His interests include 3D-DRAM, reliable memory design, and processing-in-memory (PIM). In addition, he has currently served as a Technical Program Committee member of Symposium on VLSI Circuits since 2012.



**Bongjoon Hyun** received the B.S. degree in mechanical engineering and the M.S. degree in creative IT engineering from Pohang University of Science and Technology (POSTECH), Pohang, South Korea, in 2016 and 2018, respectively, and the Ph.D. degree in electrical engineering from the Korea Advanced Institute of Science and Technology (KAIST), Daejeon, South Korea, in 2025. He is currently a Staff Engineer at Samsung Electronics. His research interests include Processing-in-Memory (PIM) architectures for AI systems, with a specific focus on Large Language Model (LLM) serving systems.



**Suk-ju Kang** (Member, IEEE) received the B.S. degree in electronic engineering from Sogang University, Seoul, South Korea, in 2006, and the Ph.D. degree in electrical and computer engineering from the Pohang University of Science and Technology, Pohang, South Korea, in 2011. From 2011 to 2012, he was a Senior Researcher with LG Display Co., Ltd., Seoul, where he was a Project Leader for resolution enhancement and multiview 3-D system projects. From 2012 to 2015, he was an Assistant Professor of Electrical Engineering with Dong-A

University, Busan, South Korea. He is currently a Professor of Electronic Engineering with Sogang University, Seoul. His current research interests include computer vision, image analysis and enhancement, video processing, multimedia signal processing, digital system design, and deep learning. He was a recipient of the IEIE/IEEE Joint Award for Young IT Engineer of the Year in 2019 and the Merck Young Scientist Award in 2022. He served as an Associate Editor for IEEE Transactions on Circuits and Systems for Video Technology from 2023.

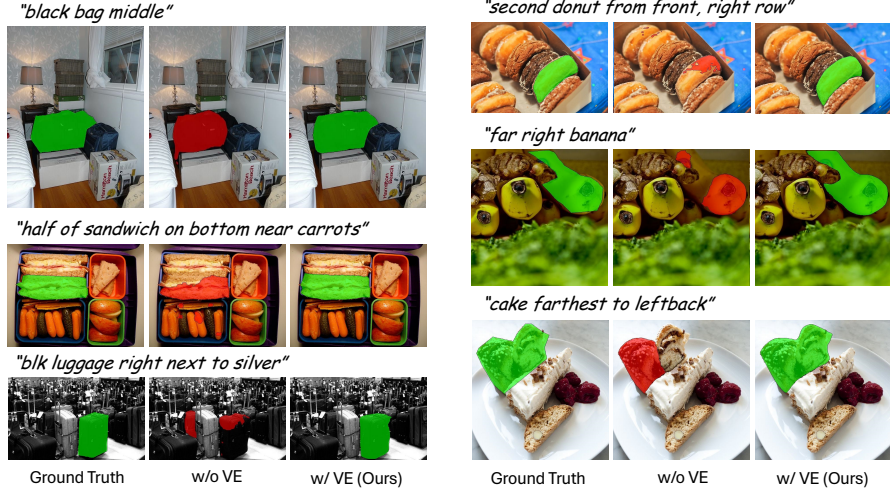


Fig. 8: Additional visualization comparison of our method and the ablated method on various target object categories, where the ablation model misses the target regions.



Fig. 9: Additional visualization comparison of our method and the ablated method on various target object categories, where the ablation model segments even non-target regions.

## APPENDIX

In Figs. 8, 9 and 10, we visualized the additional comparisons of our method and the ablated method, which uses the advanced language expression as a key-value set in the Transformer-based segmentation decoder, on various scenarios. The ablated model segment non-target region or misses the target region, whereas our visual expression method effectively segmented the target region. In Fig. 11, we compared our method with previous Transformer-based RIS approaches that exploit advanced language tokens as a key-value set on diverse image and language inputs. Our approach showed clearer segmentation compared to other methods. These results indicate that our method enhances visual understanding of fine-grained target regions more effectively.



Fig. 10: Additional visualization comparison of our method and the ablated method on the target object of the person, where the ablation model fails to capture the target regions.

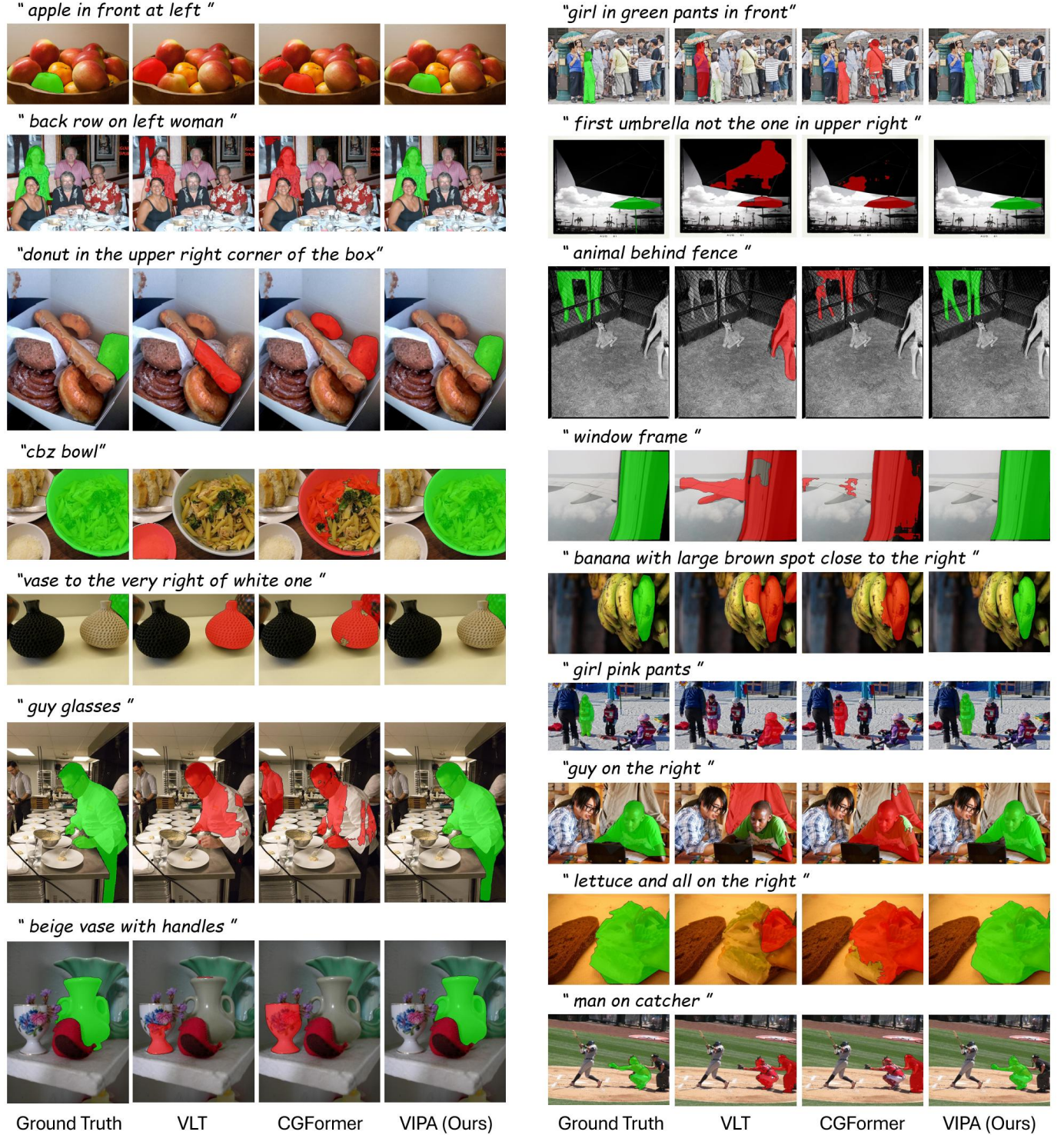


Fig. 11: Additional qualitative comparison with previous referring image segmentation models.